Proceeding of the 18th INFATS & 27th SAE-C/STC, 2024, pp1-17
2024.201

Evaluating the Protective Performance of Integrated Helmet Mask Structure under Dynamic Loads

Xuan MA[1#], Bin YANG[1*#], Feng GAO[1*#], Ronghua ZHOU[2], Jiajia ZOU[1], Xingyu ZHANG[1], Yehui SHI[3, 4]

[1]*School of Transportation Engineering, Nanjing Institute of Technology, Nanjing 211167, Jiangsu, China*

[2]*Zhiwu Yunxiang (Nanjing) Information Technology Co., Ltd., Nanjing 210031, Jiangsu, China*

[3]*Big Data Center of Jiangsu Geological Bureau, Nanjing 210007, Jiangsu, China*

[4]*Nanjing Kuntuo Civil Engineering Technology Co., Ltd., Nanjing 210000, Jiangsu, China*

Email: 15252359272@163.com, yangb123@126.com, g1850696719@163.com, 18611073228@163.com, 18105178207@163.com, 18473256993@163.com, admin@kentop.cc

[*] *Correspondence to: Bin Yang yangb123@126.com and Feng Gao g1850696719@163.com*

[#] *These authors equally contributed to this work as first author.*

Abstract: To enhance the performance of protective gear in mitigating impact-induced head injuries, a helmet mask structure composed of polycarbonate and aerogel laminated composites was designed. The Coupled Eulerian-Lagrangian (CEL) method in Abaqus was used to verify the validity of the helmet-head coupling model, and the mechanical response of different helmet mask protective structures under the action of shock waves was numerically simulated. The influence of protective structure type and thickness on head injury was analyzed. The results show that helmets with masks can delay the propagation of shock waves to the face and effectively reduce cranial stress and intracranial pressure (ICP) in the frontal and parietal lobes within 1.7 milliseconds of the shock. Specifically, the combination of polycarbonate and aerogel layers is more effective in reducing ICP in the brain compared to masks made entirely of polycarbonate. In terms of preventing moderate and severe traumatic brain injuries (TBI), the three-layer configuration with a single 0.6 mm thick aerogel layer and the five-layer configuration with double 0.6 mm thick aerogel layers offer the best protective effects. Overall, the helmet mask structure composed of polycarbonate and aerogel laminated composites can effectively reduce head injuries caused by shock waves, especially in preventing moderate and severe TBI, with the three- and five-layer configurations providing superior protection.

Keywords: helmet mask structure; aerogel; polycarbonate; protective effectiveness; shock wave load

1. Introduction

Traffic accidents are one of the leading causes of death and disability worldwide. According to a 2022 report by the World Health Organization, more than 1.3 million people die in traffic accidents each year and up to 50 million are injured [1]. Among various road users, motorcycle riders face the highest risk of accidents, with their risk of casualties being 20 times greater than that of car drivers [2]. Head injuries are particularly prevalent, accounting for up to 35% of all injuries, and often result in lifelong disabilities in motorcycle riders [3]. Therefore, it is crucial that motorcycle riders adopt effective protective measures to ensure their safety [4, 5].

Enhancing structural confinement can effectively improve the protective performance of motorcycle riders' face protection equipment, reducing the impact of shockwaves and their superimposed effects [6]. This conclusion was reached by Kang Yue et al. [7] after testing the forward and lateral shockwave protection performance of helmet-head systems with different structures and protection levels. They compared the peak shockwave overpressure and the sustained duration of action in critical areas. Valverde-Marcos et al. [8] tested riot helmets with good sealing and a double-padded structure under different shockwave loads. Their results

demonstrated that the helmet significantly lowered cerebral centroid acceleration, intracranial pressure, and cerebellar strain. Zhang et al. [9] investigated the weakening effect of the suspension liner on the head load due to shock waves using a three-dimensional head finite element model. They concluded that the foam liner could increase pulse width, delay the arrival time of the pressure peak, and reduce its impact, thus providing some protective effects for the head. Wu Yang et al. [10] conducted an experimental study on the protective performance of helmets under shockwave action. Their findings indicated that full helmets provided the best protective performance, reducing the overpressure peak by at least 80%, and that sealing performance positively impacted the shockwave protection. Rodriguez-Millan et al. [11] investigated the effectiveness of a synergistic combination of multiple protective components against generated shockwaves. The results showed that mechanisms such as adding highly confined forms of protective construction and the movement and deformation of protective equipment were effective in preventing direct injuries and reducing craniocerebral injuries. Massachusetts Institute of Technology (MIT) researchers wore a mask on a helmet to stop shockwaves from directly impacting the face, which reduced intracranial pressure by as much as 60% [12]. According to Courtney et al. [13], several transparent armor materials, including laminated glass and polycarbonate, absorb and reflect pressure to lessen the passage of shockwaves to the face. In conclusion, most recent research on head protection has focused on various helmet designs or their interior padding systems, with very little research done on the use of aerogels and their composites in the structural design of helmet masks.

This study evaluates the effectiveness of a polycarbonate-aerogel laminate composite helmet mask in reducing impact-related head injuries. To investigate the influence of different helmet mask types and thicknesses on protective performance, the mechanical response of the head to impact waves is analyzed using a validated helmet-head coupling model. The evaluation indexes include intracranial pressure (ICP), cranial stress, air pressure near the face, and mask deformation.

2. Models and methods

2.1 Finite element models

2.1.1 Head-helmet model

As shown in Figure 1(a), the head model includes the face, cortical bone, trabecula, cerebellar falx, cerebrospinal fluid, scalp, brain, cerebellum, and tentorium. Due to the highly folded nature of the meninges, scalp, and face, a tetrahedral grid is used for these components, while a hexahedral grid is utilized for the rest. In impact simulations, the face may affect the entry of shock waves into the cranial cavity. Therefore, this simplified model modifies the facial anatomical features to better fit the simulation. The validity of the coupled head-helmet model is verified using the Coupled Eulerian-Lagrangian (CEL) method in Abaqus.

The face may influence how shock waves enter the cranial cavity during impact simulations. To better fit the simulation, the simplified model adjusts the anatomical features of the face. The validity of the head-helmet coupling model was verified using the Coupled Eulerian-Lagrangian (CEL) approach in Abaqus. Research has shown that the interior padding system can reduce the number of shock waves entering the head area and mitigate the impact on the head. Different interior padding systems have varying degrees of effectiveness [14-15]. In the meshing process, a hexahedral mesh is used for the helmet and backrest, while a tetrahedral mesh is employed for the straps.

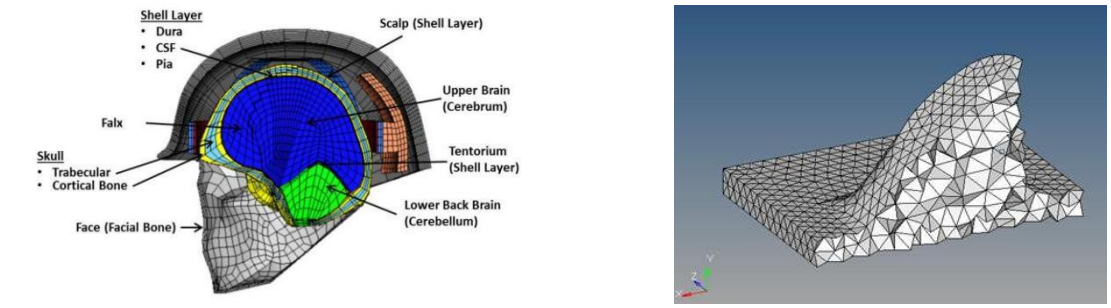

(a) Head model anatomy and helmet model interior padding system

(b) Neck device with tetrahedral mesh

Figure 1. Head and neck model

In the head model, to prevent excessive twisting and deformation of the neck's soft tissue material and to ensure the neck remains rigid, thus blocking shock waves from entering the cranial cavity from the back or underside of the head, the neck model is created in SolidWorks and then imported into Hypermesh, a finite element preprocessing program. A tetrahedral mesh is utilized for the neck model. Figure 1(b) displays the finite element model of the head and neck assembly. This design ensures that, under impact loading, the relatively soft material properties do not excessively deform the facial features and that excessive shock waves do not enter the cranial cavity, thereby preserving the accuracy of the results. The original single-layer shell unit of the model face has been remodeled. It now includes two units: a five-layer unit with a total thickness of 5 mm below the zygomatic bone and a three-layer unit with a total thickness of 3 mm above the zygomatic bone.

2.1.2 Mask model

The structure of the mask is shown in Figure 2(a) and consists of two main components: (1) a bracket, which is placed in the front area of the helmet, and (2) a protective mask with a thickness of 3 mm, which is attached to the bracket. The primary purposes of the mask are to absorb some of the impact energy, lessen the effect of shock waves on the head, and distribute the majority of the impact force away from the face. With complete coverage of the facial area and a seamless transition to the front profile of the helmet, these components were precisely modeled in SolidWorks software before being translated to the Hypermesh platform for meshing. Due to the mask material's exceptionally high density, the mask's mesh was separated into at least three layers instead of a single layer to avoid convergence issues throughout the study. The full helmet model with the mask is shown in Figure 2(b), with the mask weighing a total of 511 grams.

(a) Mask construction

(b) Model of a complete helmet with mask

Figure 2. Mask and helmet model

2.1.3 Material properties

Table 1 presents the material properties for each tissue structure. The mask consists of a laminated composite material made of polycarbonate and aerogel, with the aerogel layer sandwiched between layers of polycarbonate. The neck material is classified as soft tissue, and the facial support is constructed from aluminum. All component materials are characterized by linear elasticity and isotropy, except for the helmet material, which is defined as anisotropic [16-18].

Table 1. Component material properties

Component	Density /(kg/m^3)	Young's modulus E/(MPa)	Poisson's ratio	Bulk modulus
Bone cortex	2000	15000	0.22	-
Cerebro-Spinal Fluid	1040	0.15	0.499989	-
Endocranium	1140	31.5	0.45	-
Face	2500	5540	0.22	-
Cerebellar falx	1140	31.5	0.45	-
Hindbrain	1040	0.123	0.49	-
Neck (soft tissues)	1060	110	0.45	-
Ligament	1130	11.5	0.45	-
Scalp	1130	16.7	0.42	-
Aponeurosis	1140	31.5	0.45	-
The cerebellum	1300	1000	0.24	-
brain	1040	2.19	0.4996	-
Rear liner (polyurethane)	1600	57	0.24	-
Helmet	1230	20000/20000/7000	0.33/0.33/0.77	0.77/2.715/2.715
Leather inner belt	1153	500	0.3	-
Nylon Polyester Tape	1160	2400	0.35	-
Bracket (aluminium)	2700	70000	0.35	-
Mask (polycarbonate layer)	1220	2400	0.37	-
Mask (aerogel layer)	1000	10	0.2	-

2.2 Boundary conditions

Assuming the test item face serves as the shockwave's initiation point, a non-reflective boundary condition is applied to all surfaces (blue surfaces) in this study, except for the front side of the cube region housing the helmet model. This condition creates suction during the negative pressure phase to draw air back to the impact source, thereby simulating the air pressure distribution generated by the shock wave [19]. Because the head and helmet models are lighter than the rest of the body, the pressure from the impact loads during the analysis could cause the model to experience displacements and accelerations that differ from reality. To address this, the simulation prevents shoulder rotations and displacements by imposing boundary conditions on the neck.

2.3 Load conditions

This study assumes that the shock waveform characteristics generated by impact can be approximated by the

Friedlander waveform equation [20].

$$P = P_s e^{-(\frac{t}{t^*})}(1 - \frac{t}{t^*}) \quad (1)$$

Where P_s is the peak pressure, t^* is the time when the pressure first crosses the horizontal axis (before the negative phase).

A peak overpressure of 1 atmosphere was applied, occurring at 0.05 ms. According to the aforementioned equation, the positive pressure will gradually decrease, transitioning to a negative phase at approximately 0.15 ms, and will continue for the remainder of the pulse, ending around 0.85 ms. This loading condition is applied to the entire front surface of the cube, enabling the simulation of a planar impact.

2.4 Simulation cases

For this study, a total of five scenarios with a runtime of two milliseconds each are established. In all but one of the head models, the material and structure of the mask are modified; the remaining head model without a mask. While the thicknesses of the aerogel and polycarbonate layers vary depending on the scenario, their combined thickness remains constant at 3 mm, as detailed in Table 2.

Table 2. List of simulation cases

Cases	Helmet type	Note
1	Without a mask	
2	With polycarbonate mask	Single-layer configuration
3	With a 0.6 mm aerogel layer cover	three-Layer configuration
4	With a 1.2 mm aerogel layer cover	three-Layer configuration
5	With two 0.6 mm aerogel layer covers	five-layer configuration

3. Analysis and discussion of results

In this research, three distinct cutting planes are utilized, based on the finite element models, boundary conditions, and scenarios mentioned above. As shown in Figure 3(a), the planar "A" cut provides an axial view from the top for examining the interaction of the shock wave with the helmet, its interior padding system, and the head. A sagittal incision will be employed to evaluate a side perspective of the contour. Plane "B" cutting allows for a deeper understanding of how the shock wave interacts with the mask and face.

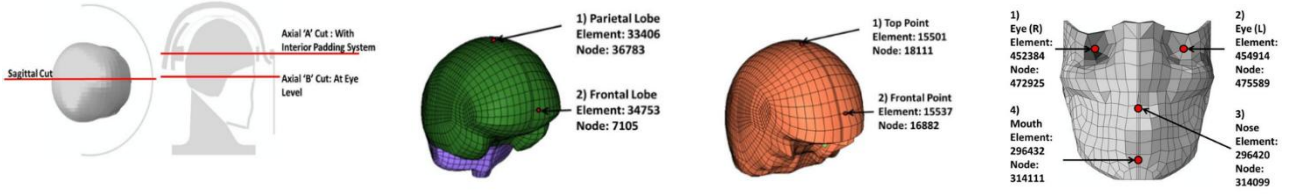

(a) Planar cuts for coronal view impact sequences

(b) ICP assessment node

(c) Skull stress assessment node

(d) Near-surface air pressure evaluation node

Figure 3. Measuring the node position

During the investigation, two distinct locations in the brain's frontal and parietal lobes are randomly selected to

assess the impact on intracranial pressure. Regarding the skull, as illustrated in Figures 3(b) and 3(c), the von Mises stresses at the anterior and vertex positions are measured to examine the impact strength of the skull. Lastly, as shown in Figure 3(d), air pressure readings are collected at four distinct locations near the face to investigate the effect of air pressure on the mouth, nose, and eyes.

3.1 Response analysis without a facemask

The focus of this study is the parametric analysis of the helmet model with a mask. To ensure the accuracy of the results, it is essential to compare the simulation results of the helmet model without mask to other simulation results that incorporate an air pressure peak overpressure impact load.

3.1.1 Shock wave propagation process

The air pressure around the helmet model changes when shock waves propagate, as illustrated in Figure 4(a). Air pressure above 0.5 MPa is indicated in red, while air pressure near ambient or negative pressure is indicated in blue. According to the analysis results, a shock wave reaches the face at 0.20 ms. Simultaneously, the shock wave in front of the helmet begins to reflect, and the amount of shock wave reflected from the helmet can be clearly seen after 10 ms, indicating that the shock wave does not directly impact the skull.

As shown in Figure 4(a), the shock wave also concentrates under the chin, bypassing the head and causing a secondary impact on the hindbrain and occipital lobe between 0.70 ms and 0.85 ms. Additionally, the shock wave enters the helmet through the earmuff portion, resulting in a high concentration of air pressure in the temporal region. At 1.05 ms, the shock wave starts to return to the front due to the negative pressure generated by the shock loading action, causing the surrounding air to be sucked forward.

3.1.2 Intracranial pressure and cranial stress

High pressure first emerges in the temporal lobe at approximately 0.350 ms, as illustrated in Fig. 4(b), and it does not develop in the frontal lobe until around 0.550 ms. Between 0.550 ms and 0.925 ms, there is a significant transfer of intracranial pressure (ICP) from the frontal brain to the occipital cortex.

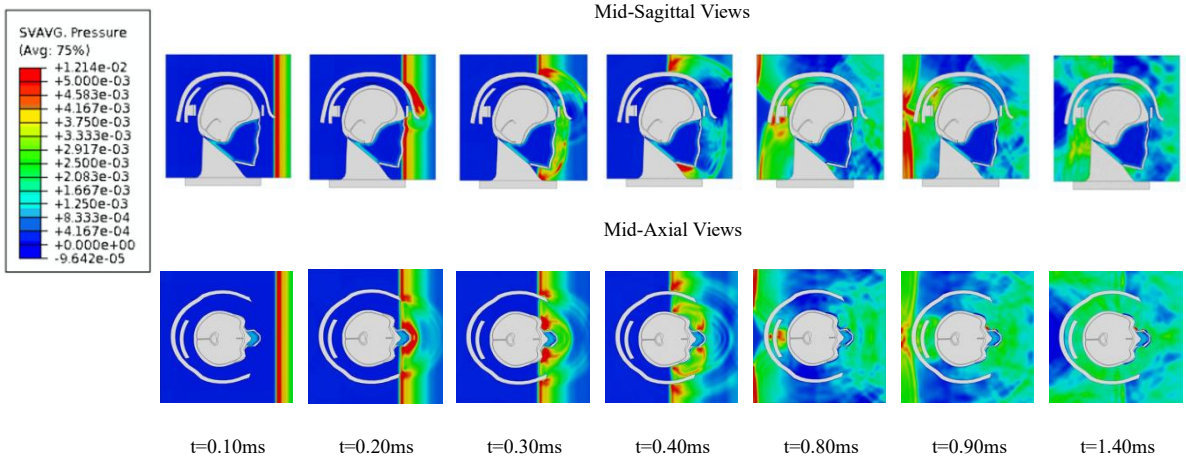

(a) Shock wave propagation without mask

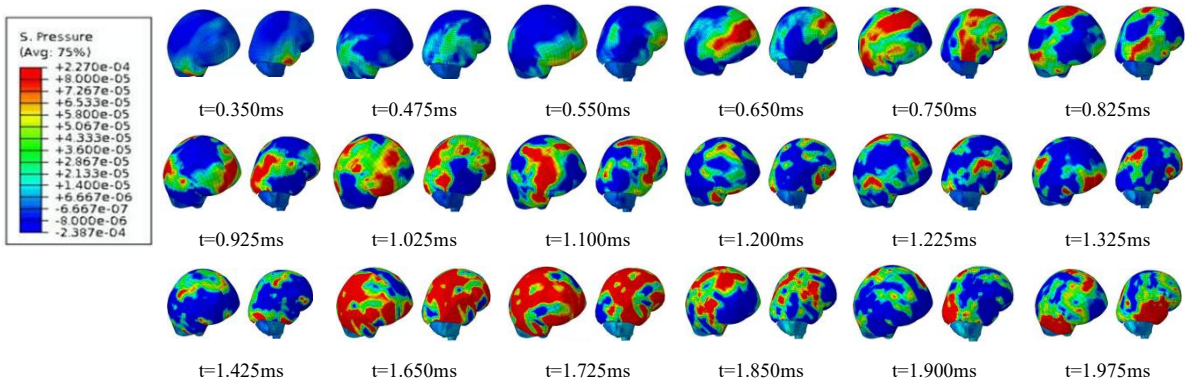

(b) ICP profile of the without mask model

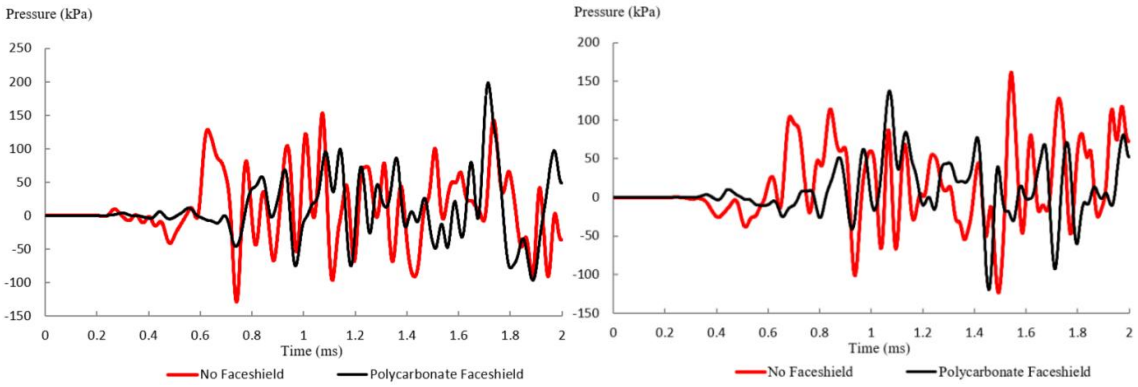

(c) Comparison of frontal and parietal lobes with and without mask intracranial pressure

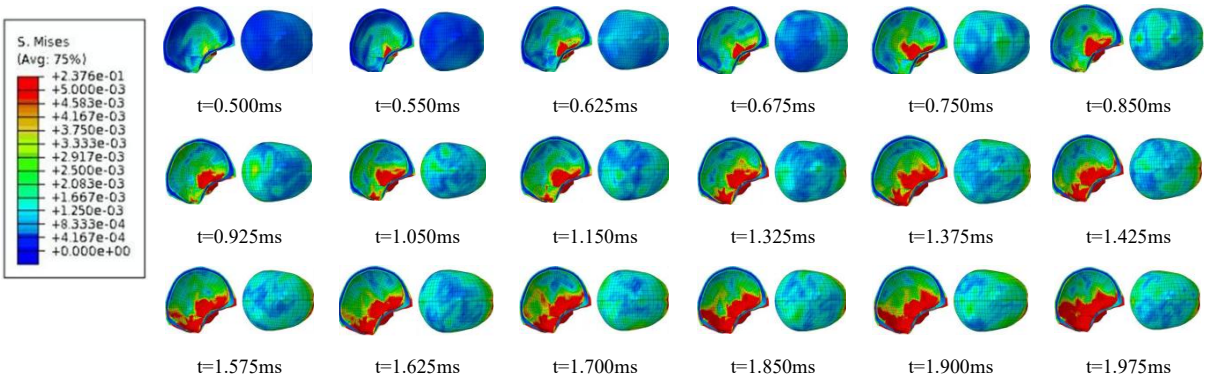

(d) Stress diagram of skull without mask

Figure. 4 Intracranial pressure, cranial stress map without mask

The ICP curves for the model without mask is depicted in Figure 4(c). At about 0.6 ms, the initial ICP in the frontal lobe is up to 0.122 MPa. During the simulation run, the frontal lobe undergoes several peaks of positive and negative pressure exceeding 0.1 MPa, and the parietal lobe exhibits a similar pattern. Since the ICP plot indicates that the shock wave travels from the front to the back of the brain, Figure 4(c) also illustrates the time delay of the initial positive pressure peak, indicating that the shock wave moves from the frontal to the parietal lobes in about 0.08 ms. Figure 4(d) shows that stress propagates from the anterior to the posterior part of the skull between 0.500 ms and 1.050 ms, then returns to the anterior at 1.150 ms due to air inhalation. High-stress regions are located on the lateral side of the skull, commencing at the bottom front and terminating at the bottom end.

3.1.3 Validation of results

The maximum values of cranial stress and the peak ranges of ICP were compared with those from previous investigations to validate the results. The ranges of the frontal and parietal ICP values are, respectively, -0.119 MPa to 0.154 MPa and -0.119 MPa to 0.161 MPa. Previous research has shown that minor variations in the head model's geometry, the arrangement of the helmet's interior padding, and the material composition can affect the values of cranial stress and ICP [17–18].

A study by Grujicic et al. [19] involving a 0.1MPa (1 atm) peak overpressure impact recorded ICP values between -0.08 MPa and 0.08 MPa in their helmet model. Another study by Zhang et al. [20] found that the peak ICP for a 0.27 MPa (2.7 atm) peak overpressure impact in a helmeted condition was 0.6 MPa. In this study, the stress at the front and top of the skull was found to be 4.37 MPa and 2.71 MPa, respectively. Tan et al. [17] conducted a study also based on a 0.1 MPa peak overpressure, with their simulation results showing skull stress values of 6 MPa and 11 MPa for two different helmet configurations.

3.2 Model response analysis with mask

3.2.1 Shock wave propagation process

The shock wave begins to impact the mask at 0.10 ms, as shown in Figure 5(a). Between 0.20 ms and 0.30 ms, the mask prevents the shock wave from directly striking the face. However, due to its limited thickness and short length, the mask cannot stop the diffracted shock wave from reaching the face. The mask diffracts most of the shock wave and delays its entry into the helmet earmuffs from 0.10 ms to 0.65 ms, compared to the scenario without the mask. The area of high pressure between the head and the helmet is significantly reduced with the mask, and there is also less secondary impact on the occipital lobe when comparing the air pressure profiles during these intervals. However, over time, the negative pressure generated by the impact loading effect causes air to be drawn in, accumulating high pressure between the mask and the face and reflecting it multiple times for a duration that may exceed 2 ms.

3.2.2 Intracranial pressure and cranial stresses

The initial ICP values in the temporal lobe decrease from 0.350 ms to 0.475 ms when the mask is present, as shown in Fig. 5(b). Additionally, the intracranial pressure in the frontal lobe is notably lower in the no-mask scenario compared to the frame at 0.650 ms. However, with a mask, elevated ICP is observed in the frontal and temporal lobes between 1.900 ms and 1.975 ms. This may be due to the accumulation and repeated reflection of stagnant air between the face and the mask.

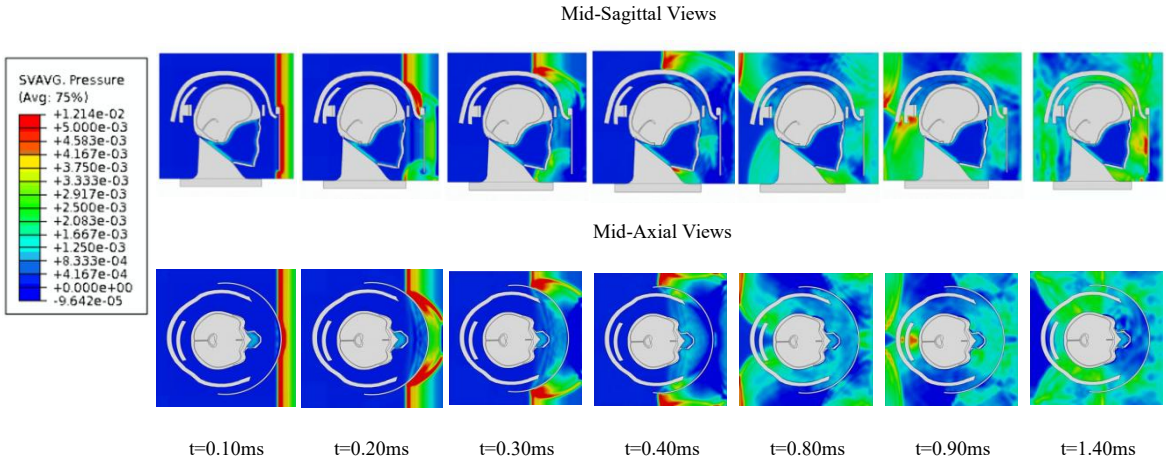

(a) Shock wave propagation with mask

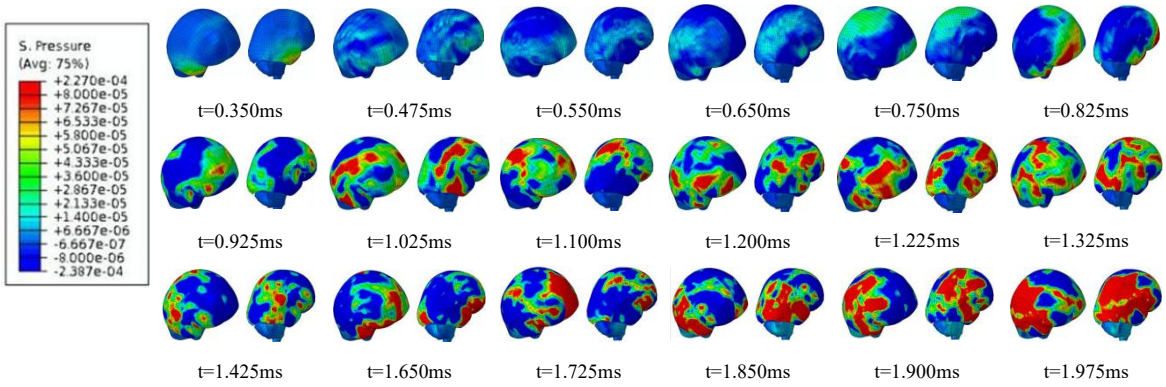

(b) ICP profiles with mask

Figure 5. Shock wave propagation with mask

As shown in Table 3, although the mask is able to diffract the shock wave and significantly reduce the ICP at 0.61 ms (the initial overpressure peak in the condition without mask), the ICP while wearing a mask is still higher and appears after 1.71 ms. This is because at approximately 1.50 ms, the inhalation shock wave and diffraction wave depicted in Figure 5(b) start to generate structural disturbances near the helmet's ear. These amplified shock waves then propagate forward and severely damage the frontal lobe. Altering the mask's size (e.g., extending the side edges of the mask) can prevent these structural disturbances. As shown in Table 4, the amplification effect of the shock wave does not appear to reach the parietal lobe. In the case of wearing a mask, the maximum and minimum ICP values in the parietal lobe are lower, indicating that the stress caused by the structural disturbance is concentrated behind the parietal lobe.

The first peak stress of the mask model was lower in both skull positions compared to the case without the mask, suggesting that the mask's ability to diffract waves helped lessen the impact of shock waves on the skull. However, it is evident that the face mask causes more stress at the front end, with the maximal stress in both locations occurring after 1.91 ms. As seen in Fig. 6(a), this might be due to the buildup of air pressure between the mask and the face.

From the stress wave propagation shown in Figure 6(a) and Figure 6(b), the propagation direction and intensity appear similar in both cases. However, when wear a mask, the pressure on the skull side is reduced. The analysis results depicted in Figure 6(b) are detailed in Table 5 and Table 6.

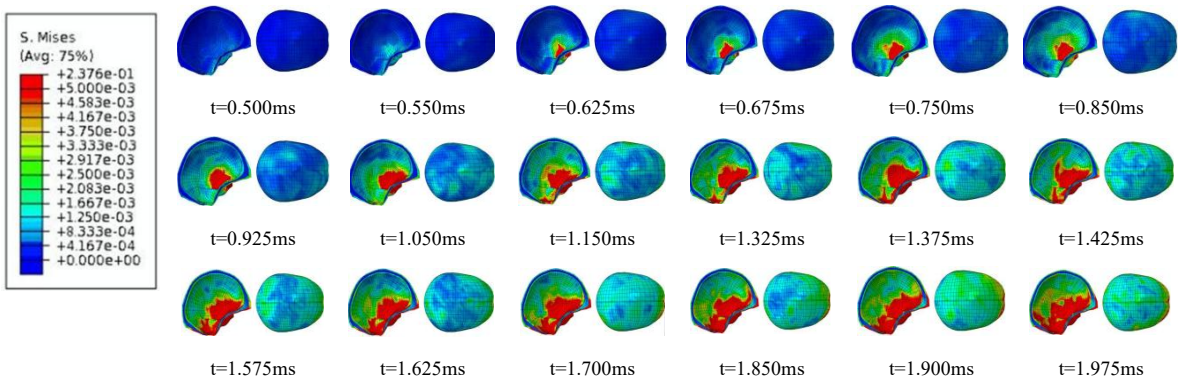

(a) Cranial stress maps for models with mask

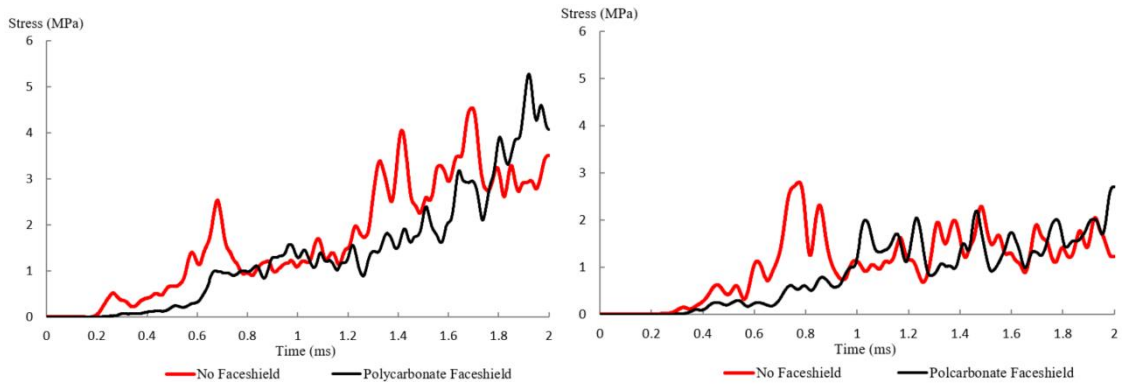

(b) Comparison of skull stress between anterior points and apex with or without mask

Figure. 6 Intracranial pressure, cranial stress map without mask

Table 3. Frontal intracranial pressure

Frontal intracranial pressure	Maximum pressure (10^{-3}MPa)	Period of time (ms)
Without mask	154	1.54
Polycarbonate mask	194	1.71

Table 4. Parietal intracranial pressure

parietal intracranial pressure	Maximum pressure (10^{-3}MPa)	Period of time (ms)
Without mask	161	1.54
Polycarbonate mask	134	1.07

Table 5. Cranial anterior point stresses

Cranial anterior point stress	Maximum pressure (MPa)	Period of time (ms)
Without mask	4.37	1.68
Polycarbonate mask	5.18	1.91

Table 6. Stresses on the top of the skull

Cranial vertex stress	Maximum pressure (MPa)	Period of time (ms)
Without mask	2.71	1.54
Polycarbonate mask	2.59	2.00

3.2.3 Facial air pressure

As shown in Figure 7, between 0.2 ms and 0.4 ms, the mask diffracted the shock wave upon impact with the model, significantly reducing the air pressure near three key points on the face.

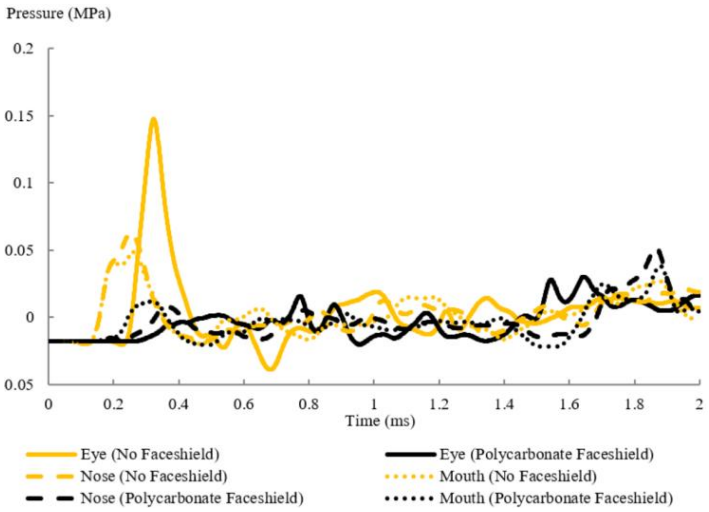

Figure.7 Comparison of air pressure underneath the mask with and without mask

3.3 Response analysis of different protective masks

3.3.1 Intracranial pressure and cranial stresses

As observed in the graphs in Fig. 8(a) and Fig. 8(b), the intracranial pressure in the frontal and parietal lobes of all structures is identical until 0.9 ms. Once the impact load front has passed through the head, the pressure is drawn back by the ensuing negative pressure.

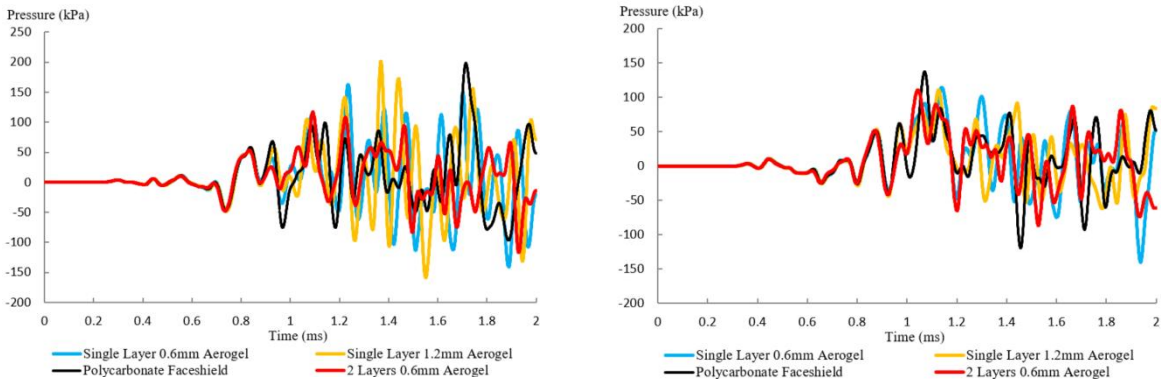

(a) Frontal intracranial pressure

(b) Parietal intracranial pressure

Figure 8. Frontal and parietal intracranial pressures for different mask configurations

As shown in Table 7, a fully polycarbonate mask (without aerogel) can delay the gas build-up time but will ultimately lead to an increase in intracranial pressure (ICP) in the frontal lobe. Additionally, a single-layer 0.6 mm aerogel mask outperforms a single-layer 1.2 mm aerogel mask. However, when the 1.2 mm aerogel layer is split into double 0.6 mm layers and arranged in a five-layer structure, it demonstrates superior performance in mitigating shock wave effects.

Table 7. Frontal ICP for different mask configurations

Type	Maximum pressure (10^{-3}MPa)	Period of time (ms)	Minimum pressure (10^{-3}MPa)	Period of time (ms)
Polycarbonate masks	194	1.71	-85	1.87
Single layer 0.6 mm aerogel	159	1.23	-132	1.88
Single layer of 1.2 mm aerogel	201	1.37	-154	1.55
Double layer 0.6 mm aerogel	110	1.09	-135	1.88

Table 8 indicates that the maximum pressure for both the single-layer 1.2 mm aerogel mask and the double-layer 0.6 mm aerogel mask is the same, with the lowest pressure observed at the parietal lobe position. When comparing three-layer masks, the thicker aerogel layer performs better in the parietal lobe than in the frontal lobe. However, a mask combining aerogel with a fully polycarbonate mask more effectively reduces impact load-induced ICP in both the frontal and parietal lobe regions.

Table 8. Parietal ICP for different mask configurations

Type	Maximum pressure (10^{-3}MPa)	Period of time (ms)	Minimum pressure (10^{-3}MPa)	Period of time (ms)
Polycarbonate masks	133	1.07	-116	1.44
Single layer 0.6 mm aerogel	114	1.14	-133	1.93
Single layer of 1.2 mm aerogel	104	1.12	-56	1.79
Double layer 0.6 mm aerogel	104	1.04	-80	1.51

According to Figures 9(a), 9(b), and Table 9, a thinner aerogel layer (0.6 mm) more effectively mitigates the impact at the anterior point, while a thicker aerogel layer (1.2 mm) better reduces the impact at the apex. The stress at the anterior point of the skull is more effectively reduced by a double-layer 0.6 mm aerogel mask, whereas the stress at the apex is more significantly diminished by a single-layer 1.2 mm aerogel mask.

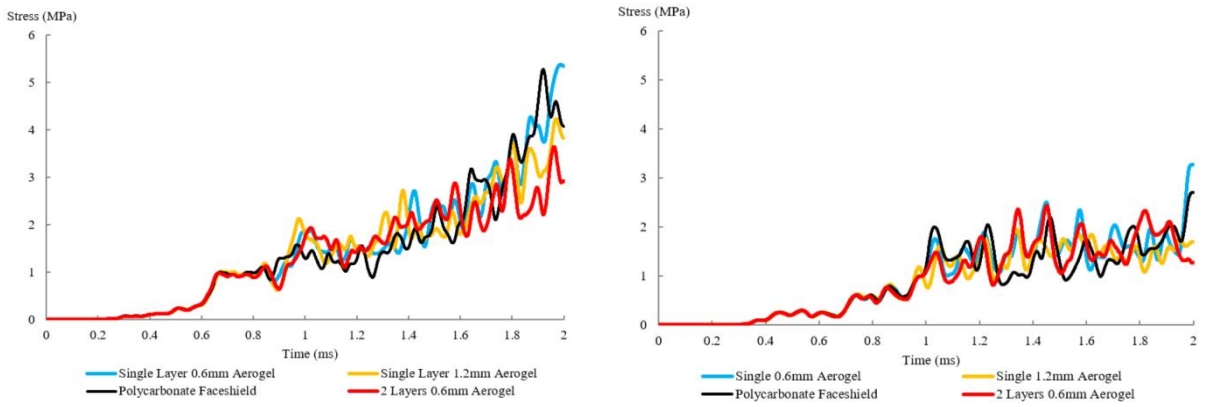

(a) Skull stress at the anterior point

(b) Skull stress at the cranial point

Figure 9. Anterior and vertex cranial stresses in different mask configurations

Table 9. Cranial stresses for different mask configurations

	Maximum stress at the front point (MPa)	Period of time (ms)	Maximum Vertex Stress (MPa)	Period of time (ms)
Polycarbonate masks	5.18	1.91	2.59	2
Single layer 0.6 mm aerogel	5.28	1.97	3.19	1.98
Single layer of 1.2 mm aerogel	4.34	1.95	1.36	1.83
Double layer 0.6 mm aerogel	3.63	1.95	2.299	1.44

3.3.2 Facial air pressure

With the exception of the fully polycarbonate mask, all controls exhibited similar air pressure at the mouth and nose, as shown in Figures 10(a) and 10(b). However, as illustrated in Figure 10(c), the mask structure significantly affected the air pressure at the eyes. Table 10 reveals that the single-layer 1.2 mm aerogel mask recorded the lowest maximum air pressure, more effectively diffracted the shock wave, and resulted in air accumulation between the mask and the face at approximately 1.65 ms. Furthermore, it was observed that the double-layer 0.6 mm aerogel mask showed maximum and minimum pressures at intervals of 0.85 ms and 1.10 ms, respectively. In contrast, other masks did not exhibit these pressure variations until the air pressure inside the mask started to increase. This difference might indicate that the five-layer structure resulted in lower ICP and cranial stresses due to its greater effectiveness in diffracting the stronger frontal shock wave.

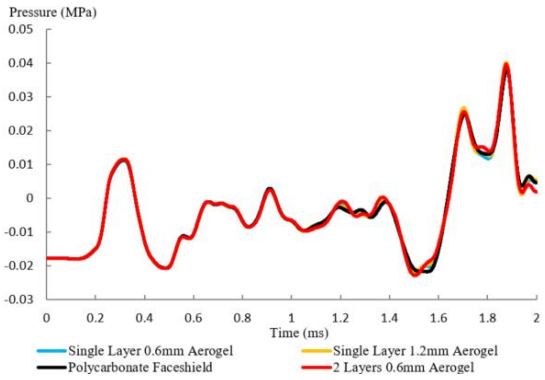

(a) Air pressure near the mouth

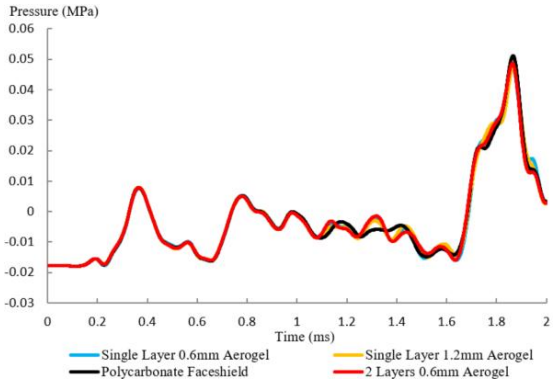

(b) Air pressure near the nose

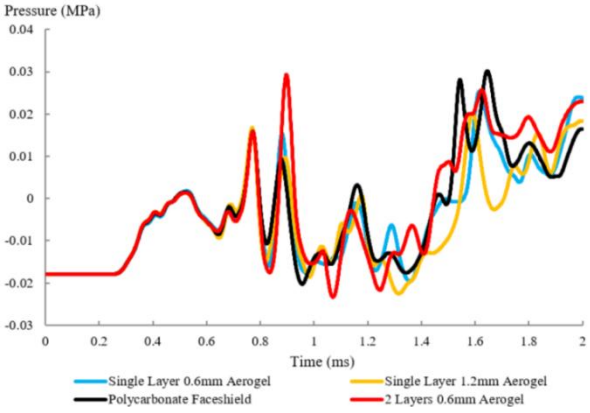

(c) Air pressure near the eyes

Figure 10. Air pressure at different parts of the attachment for different mask configurations

Table 10. Air Pressure near the eye for mask configuration

Air pressure near the eyes	Maximum pressure (MPa)	Period of time (ms)	Minimum pressure(MPa)	Period of time (ms)
Polycarbonate masks	0.029	1.64	-0.019	0.94
Single layer 0.6 mm aerogel	0.023	1.97	-0.020	1.34
Single layer of 1.2 mm aerogel	0.019	1.58	-0.022	1.29
Double layer 0.6 mm aerogel	0.028	0.89	-0.025	1.06

3.3.3 Mask deflection

An essential measure of a mask's overall stiffness and shock-absorbing capacity is its deflection. Furthermore, the degree of deflection influences how the shock wave disperses from the critical areas of the skull. Therefore, studying the role of mask deflection in reducing shock loads is crucial. Figure 11 shows the amount of deflection for three different mask configurations. At 0.30 ms and 0.70 ms, deflection occurs at the center of the mask, followed by significant deformation at the bottom. At 1.00 ms, high deflection is observed at the location where the mask aligns with the eyes. From 1.40 ms onwards, inward deflection occurs across the mask, with the highest deflection again occurring at the bottom. According to the deflection contours, two high-deflection points are identified, as shown in Figure 12(a), indicating that the maximum deflection occurs at the second point at the bottom of the mask. Based on the cantilever bending hypothesis, this finding suggests that the highest deflection happens farthest from the fixed point. Point 2 was used as an example to measure mask deflection, with the findings displayed in Figure 12(c). The figure shows that the deflection pattern is consistent across all configurations, with maximum deflection occurring around 0.6 ms. The deflection decreases between 0.60 ms and 0.95 ms, aligning with the shock wave propagation in Figure 5(a), where the shock wave is diffracted by the mask, thereby lessening the pressure exerted on it. The mask then deflects inward again between 1.00 ms and 1.30 ms, coinciding with the presence of negative pressure at the impact load's center, which pulls air in front of the mask. Simultaneously, the air flowing through the model is drawn towards the mask by the negative pressure, resulting in a decrease in deflection.

By comparing the graphs of the different mask structures, it can be concluded that the single-layer 0.6 mm aerogel mask exhibits the lowest peak deflection, indicating that this material is the stiffest. This stiffness may also explain the relatively high ICP and cranial stresses associated with this construction, as the rigid mask allows air pressure to build up between the face and the mask before entering the cranial cavity. Furthermore, the deflection behavior of the five-layer structural mask appears erratic between 1.2 ms and 2.0 ms, with the lowest deflection occurring between 1.2 ms and 1.6 ms and the highest deflection occurring between 1.6 ms and 2.0 ms. During these intervals, the amount of deflection varies more significantly than in the three-layer structure. The shock wave diffracts differently depending on the degree of deflection, thereby improving shock mitigation to the frontal, parietal, and anterior regions of the skull.

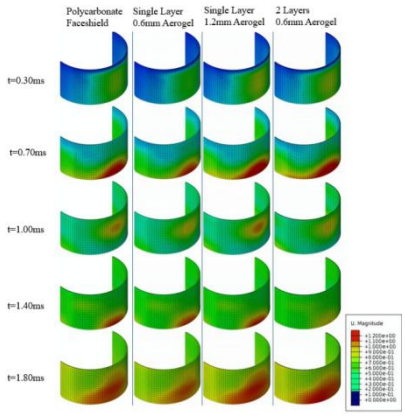

Figure 11. Inward deflection profile on shield for different shield configurations

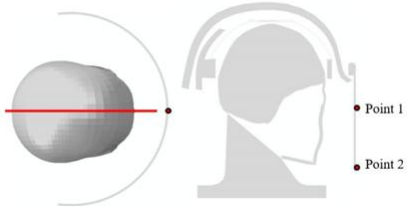

(a) Deflection point on the mask

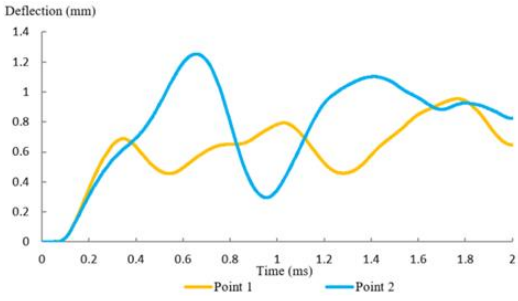

(b) Single 0.6 mm aerogel mask deflected inwards at points 1 and 2

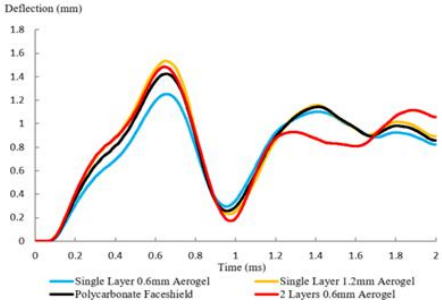

(c) Inward deflection of different mask structures at point 2

Figure. 12 Pressure at different deflection points on the mask

4. Conclusions

Through numerical simulation, the protective effects of polycarbonate and aerogel helmet mask structures under shock waves were investigated. The validity of the head-helmet coupling model was confirmed by comparing it with experimental data from the literature, leading to the following conclusions:

(1) Response evaluations comparing helmet models with and without a 3 mm polycarbonate mask revealed that the inclusion of a mask effectively lowered the frontal lobe's ICP from the start of the impact until 1.5 ms. After this point, the impact's negative pressure caused gases to be drawn in and accumulate between the face and the mask, resulting in higher ICP values compared to scenarios without a mask. This behavior was also observed in research examining the impact's influence on the cranium; the same phenomenon was noted when assessing bomb impact effects on the skull. However, the mask significantly reduced pressure in the vicinity of the face and the parietal lobe.

(2) Using a single layer of 0.6 mm thick aerogel, a single layer of 1.2 mm thick aerogel, and a double layer of 0.6 mm thick aerogel sandwiched between polycarbonate layers, the total thickness of the mask reached 3 mm. Numerical simulation results showed that increasing the thickness of the aerogel in the three-layer mask structure more effectively

alleviated air pressure in the parietal lobe, at two skull observation points, and near the eyes. Furthermore, the facemask's ability to deflect and diffract shock waves made the five-layer configuration—comprising double layers of 0.6 mm aerogel—the most effective in reducing the effects of shock loading on the frontal, parietal, and anterior parts of the skull. In terms of lowering frontal and parietal ICP, the combination of polycarbonate and aerogel layers performed better than a solid polycarbonate mask.

(3) According to the ICP tolerance threshold standard, severe TBI occurs when the maximum ICP exceeds 0.235 MPa, while mild or no TBI occurs when the ICP is below 0.173 MPa [21]. The analysis results indicated that under a 0.1 MPa shock, severe TBI occurs without mask protection, and complete polycarbonate masks or single-layer 1.2 mm aerogel masks result in moderate TBI. In contrast, using a combination mask with a three- or five-layer structure, or redesigning the end of the mask to disperse the shock wave and avoid barometric pressure build-up, can minimize the brain damage caused by shock loading.

Authors contributions

XM, BY, FG and RZ: Conceptualization, Methodology, Software, Writing - original draft preparation, Visualization. JZ, XZ and YS: Conceptualization, Investigation, Validation, Writing - review & editing, supervision. All authors contributed to the article and approved the submitted version. XM, BY, FG and RZ are co-first authors and contributed equally to this study.

Acknowledgement

We appreciate the editors and referees for their valuable remarks and advice, which have significantly enhanced the clarity of the paper. We would also like to express our gratitude for the financial support provided by the National Natural Science Foundation of China (Grant No. 12372079), the Natural Science Foundation of Jiangsu Province, China (Grant No. BK20201470), Nanjing University of Engineering Graduate Student Science and Technology Innovation Fund Project (No. TB202417038).

References

[1] World Health Organization. *Global status report on road safety*. 2022. Geneva: WHO Press.

[2] Liu, D., Li, Y. D., Zhao, H. and Zhu, X. *Relativity analysis of pedestrian head injuries and the headform to bonnet top test method*. Journal of Highway and Transportation Research and Development, 2004, **1**: p. 98-101, 105 (in Chinese).

[3] Liu, Z. L, Du, Z. B., Zhang, J. R, et al. *Progress in the mechanism and protection of blast-induced traumatic brain injury*. Explosion and Shock Waves, 2022. **42**(4): 041101.

[4] Li, C. Z., Wang, Y. J. *Progress in the study of blast shockwave brain injury*. Clinical Journal of Medical Officer, 2010. **38**(2): p. 311–315.

[5] Yudhijit, Bhattacharjee, Neuroscience. *Shell shock revisited: solving the puzzle of blast trauma*. Science, 2008. 319(5862): p. 406-408.

[6] Arregui-Daimasesc, C., Lopez-Valdes, F. J. and Segui-Gomez, M. *Pedestrian injuries in eight European countries: An analysis of hospital discharge data*. Accident Analysis & Prevention, 2010. **42**(4): p. 1164-1171.

[7] Kang, Y., Zhang, S. Z., Zhang, Y. P., et al. *Research on anti-shockwave performance of the protective equipment for the head of a soldier based on shock tube evaluatio*n. Explosion and Shock Waves, 2021. **41**(8): 085901.

[8] Valverde-Marcos, B., Rubio, I., Antona-Makoshi, J., et al. *Numerical analysis of EOD helmet under blast load events using human head model*. Applied Sciences, 2020, **10**(22): p. 8227.

[9] Zhang, T. G., SATAPATHY, S. S. *Effect of helmet pads on the load transfer to head under blast loadings*, Proceedings of the ASME 2014 International Mechanical Engineering Congress and Exposition. Montreal: American Society of Mechanical Engineers, 2014.

[10] Yang, W. U., Bin, Q., Shu, W., et al. *Helmet protection based on explosive shock waves*. ACTA ARMAMENTARII, 2022. **43**(9): p. 8.

[11] Rodriguez-Millanm, Tan, L. B., Tse, K. N., et al. *Effect of full helmet systems on human head responses under blast loading*. Materials & Design, 2017. **117**: p. 58–71.

[12] Nyein, M. K., Jason, A. M., Yu, L., et al. *In Silico Investigation of intracranial blast mitigation with relevance to military traumatic brain injury*. Proceedings of the National Academy of Sciences of the United States of America, 2010. **107**(48): p. 20703-20708.

[13] Courtney, E. D., Courtney, A. C., Courtney, M. W. *Blast wave transmission through transparent armour materials*. Journal of Battlefield

Technology, 2012, **15**(2): p. 19-22.
[14] Ganpule, S., Gu, L., Alai, A., et al. *Role of helmet in the mechanics of shock wave propagation under blast loading conditions*. Computer Methods in Biomechanics and Biomedical Engineering 2012, **15**: p. 1233–1244.
[15] Ganpule, S., Alai, A., Plougonven, E., et al. *Mechanics of blast loading on the head models in the study of traumatic brain injury using experimental and computational approaches*. Biomechanics & Modeling in Mechanobiology, 2012. **12**: p. 511–531.
[16] Huang, X., Zheng, Q., Chang, L., et al. *Study on protective performance and gradient optimization of helmet foam liner under bullet impact*. Scientific reports, 2022. **12**(1): 16061.
[17] Tan, L. B., Lee, H. P., Tan, B. C. V. *Performance evaluation and design improvement of interior cushioning system of ballistic helmets*. Department of Mechanical Engineering. National University of Singapore, 2012.
[18] Dewey, J. M. *The shape of the blast wave: Studies of the Friedlander equation*. 2010.
[19] Grujicic, A., Laberge, M., Grujicic, M., Pandurangan, B., et al. *Potential improvements in shock-mitigation Efficacy of a polyurea-augmented advanced combat helmet*. Journal of Materials Engineering & Performance, 2012. **21**(8): p. 1562-1579.
[20] Zhang, L., Makwana, R., Sharma, S. *Comparison of the head response in blast insult with and without combat helmet*. 2011: p. 1-18.
[21] Panzer, M. B., Matthews K, A., Yu, A. W., et al. *A multiscale approach to blast neurotrauma modeling: Part I – development of novel test devices for in vivo and in vitro blast injury models*. Frontiers in Neurology, 2012. **3**: 46.